International Journal of Heat and Technology
Vol. 42, No. 4, August, 2024, pp. 1465-1472
Journal homepage: http://iieta.org/journals/ijht

Experimental Study on the Distribution Patterns of Moisture and Temperature Fields in Highway Embankments in Cold Regions

Jiashuo Cao

College of Civil Engineering and Transportation, Northeast Forestry University, Harbin 150040, China

Corresponding Author Email: 13304659778@163.com

https://doi.org/10.18280/ijht.420436

Received: 16 April 2024
Revised: 30 June 2024
Accepted: 13 July 2024
Available online: 31 August 2024

Keywords:
cold regions, embankment, temperature field, moisture field, monitoring

ABSTRACT

In cold regions, the freezing and thawing of embankments often cause significant damage to road surfaces. Research indicates that this freeze-thaw process is closely related to the distribution of temperature and moisture within the embankment. Therefore, an in-depth study of the moisture and temperature conditions and the resulting deformation under freeze-thaw effects is fundamental for analyzing crack-related diseases in road surfaces. The authors have developed a monitoring system for moisture and temperature in cold region highway embankments to conduct long-term observations. Based on the collected data, the distribution patterns of moisture and temperature fields in the embankment were analyzed. The results indicate that temperature changes at different locations within the embankment generally correspond to atmospheric temperature changes, exhibiting a periodic sinusoidal pattern. The annual variation in embankment temperature shows a nonlinear negative correlation with depth.

1. INTRODUCTION

With the rapid development of global infrastructure construction, the unevenness of seasonal freeze-thaw damage in permafrost has attracted increasing attention from scholars. The Heilongjiang Province of China is located in a cold region, influenced by a cold temperate and temperate continental monsoon climate. Winters are long and harsh, while summers are warm and rainy. These unique climatic conditions pose significant challenges to the service life of highways [1]. The freeze-thaw of embankments is often the root cause of road surface damage, which not only greatly affects the aesthetics of the road surface and reduces driving comfort and safety but also significantly increases the economic costs of highway maintenance. Therefore, studying the moisture, temperature conditions, and deformation of the embankment under the influence of freeze-thaw is fundamental to understanding the occurrence of crack-related diseases on the road surface [2-6].

Based on the domestic and international research background, up to now, there is still insufficient analysis of the occurrence and development patterns of longitudinal cracks induced by embankment freeze-thaw under cold region climatic conditions, as well as the correlation between cracks and freeze-thaw. In terms of the environmental characteristics of asphalt pavement in cold regions, starting from the moisture, heat, and deformation of the embankment, further improvement is needed for the research on constructing a numerical model for the evolution of longitudinal cracks in asphalt pavement of highways induced by freeze-thaw in cold regions [7-15].

In the authors' previous studies, through a series of experimental analyses, the results showed a correlation between the occurrence and development of longitudinal cracks and uneven freeze-thaw of the embankment. Since embankment freeze-thaw is mainly related to the temperature and moisture distribution of the embankment, this paper relies on a highway expansion project in Heilongjiang Province. Three typical cross-sections were selected where water-temperature sensors were embedded to monitor the temperature and moisture changes of the embankment over a long period. Based on the collected data, the moisture field and temperature field of the embankment were analyzed to monitor the changes in moisture, temperature, and vertical deformation of the road surface. This also provides validation for subsequent numerical analysis in related studies. Further, in combination with the numerical simulation process, the formation and development of longitudinal cracks are summarized and analyzed to propose measures for preventing and controlling longitudinal cracks, thereby providing suggestions for highway construction and maintenance. This is of great significance for improving the service life and service level of highways.

2. OVERVIEW OF HIGHWAY ENGINEERING AND NATURAL CONDITIONS

The project for this study is a highway expansion project, conducting long-term monitoring of the moisture and temperature conditions of the embankment. The monitored section is located in the suburbs of Harbin City, China, within a typical seasonal freeze-thaw zone. The annual temperature variation in this area conforms to a sine function. Winters are cold and long, with the lowest average temperature in January reaching -17.3°C, while the highest temperature in summer occurs in July, with an average temperature of 23.5°C. The rainfall variation in this area generally follows a normal function, with low precipitation in winter and a distinct rainy season in summer. The cumulative monthly rainfall from January to March and from November to December is less than 20 mm, while the rainfall in July reaches the annual maximum of 164.5 mm. The average rainfall from June to August exceeds 120 mm.

The pavement structure of the project consists of a 22 cm asphalt concrete surface layer and a 56 cm cement-stabilized base layer. For cut sections, the lower part comprises a 20 cm asphalt milling material, a 20 cm sand cushion layer, and an 80 cm replacement soil layer, all made of clay for the subgrade part. For fill sections, the lower part includes a 20 cm asphalt milling material and a 20 cm sand cushion layer, with the subgrade part being clay.

3. LAYOUT OF THE EMBANKMENT MOISTURE-TEMPERATURE MONITORING SYSTEM

3.1 Moisture-temperature monitoring system

The moisture-temperature monitoring system mainly consists of sensors, wires, photovoltaic panels, batteries, a solar digital display controller, an IoT intelligent gateway, and data acquisition system software. The sensors are used to collect the volumetric moisture content and temperature of the embankment. The photovoltaic panels, batteries, and digital display controller form the power supply system. The IoT intelligent gateway is used for data collection, analysis, and uploading [16, 17]. The data acquisition system software is used for data storage and querying. All parts are connected using shielded wires to complete the construction of the entire moisture-temperature monitoring system. The sensors used are MS20 soil temperature and humidity sensors, which have characteristics such as high measurement accuracy, high sensitivity, and stable operation. They can simultaneously measure the temperature and volumetric moisture content of the embankment soil. The temperature measurement range of these sensors is -40 to 80°C, and the volumetric moisture content measurement range is 0 to 100%. They can be placed in a temperature environment of -40 to 85°C and be submerged in water for long periods without damage. The volumetric moisture content measurement accuracy of these sensors is ± 2% (within the 0 to 53% range) or ± 4% (within the 53 to 100% range), and the temperature measurement accuracy is ± 0.4°C. The highest data acquisition frequency can be set to 1 time/second, which fully meets the needs of moisture-temperature monitoring. Each device of this sensor type is internally marked with a unique address number. Multiple sensors are connected in parallel, and the collected data is transmitted to the IoT intelligent gateway through a main wire. The intelligent gateway can automatically identify, analyze, and upload the data to the backend server based on the address number, allowing users to view the data via mobile phone or computer.

3.2 Calibration experiment of sensors

Since the data collected by the sensor for soil moisture in the embankment is volumetric moisture content, and the mass moisture content is usually required in experimental analysis, it is necessary to convert the collected volumetric moisture content into the required mass moisture content. Additionally, there may be certain errors in the sensors' measurements of moisture and temperature. Based on these two aspects, it is necessary to conduct calibration experiments on this type of sensor [18, 19].

The calibration experiment mainly involves separately calibrating the temperature and moisture measurements of the sensors (refer to Figure 1). The calibration experiment should simulate the actual state of the embankment soil as closely as possible. That is, using raw soil used in the construction of the embankment, quicklime is mixed in at a ratio of 3% by the external mixing method. A soil column with a compaction degree of 96% or 93% is formed in a 10 cm × 10 cm mold by static compaction, and the sensor is inserted for measurement.

Figure 1. Calibration experiment of sensors

To ensure the accuracy of the moisture calibration experiment results, five soil samples with moisture contents of 15%, 18%, 21%, 24%, and 27% were prepared. Each soil sample was compacted at compaction degrees of 93% and 96%, respectively. Three sensors were selected and inserted into each soil sample for measurement, with each sensor inserted twice. The position of the sensors was adjusted during insertion to reduce errors. Therefore, for each soil sample at a specific compaction degree, six data points could be obtained through sensor measurements, and the average value was taken. A portion of the soil sample was removed and placed in an aluminum box to measure its true moisture content. The experimental results are shown in Tables 1 and 2.

Table 1. Volumetric moisture content measurements at 93% compaction degree

Soil Sample Number	Sensor 1 Measurement (%)		Sensor 2 Measurement (%)		Sensor 3 Measurement (%)		Average Value (%)
1	19.71	21.14	20.06	20.88	20.38	23.98	21.0
2	22.91	26.51	26.25	27.85	23.58	26.01	25.5
3	31.42	31.35	29.73	29.8	31.78	31.86	31.0
4	35.45	35.64	33.13	33.13	33.92	34.3	34.3
5	37.21	36.97	38.61	35.59	37.52	41.52	37.9

Table 2. Volumetric moisture content measurements at 96% compaction degree

Soil Sample Number	Sensor 1 Measurement (%)		Sensor 2 Measurement (%)		Sensor 3 Measurement (%)		Average Value (%)
1	20.94	18.61	20.47	20.88	20.83	21.98	20.6
2	24.86	23.82	26.07	23.3	25.89	25.83	25.0
3	26.38	29.93	30.01	32.36	29.73	28.52	29.3
4	33.91	35.11	35.78	36.08	35.1	35.59	35.3
5	38.52	37.35	37.67	41.07	40.98	40.44	39.3

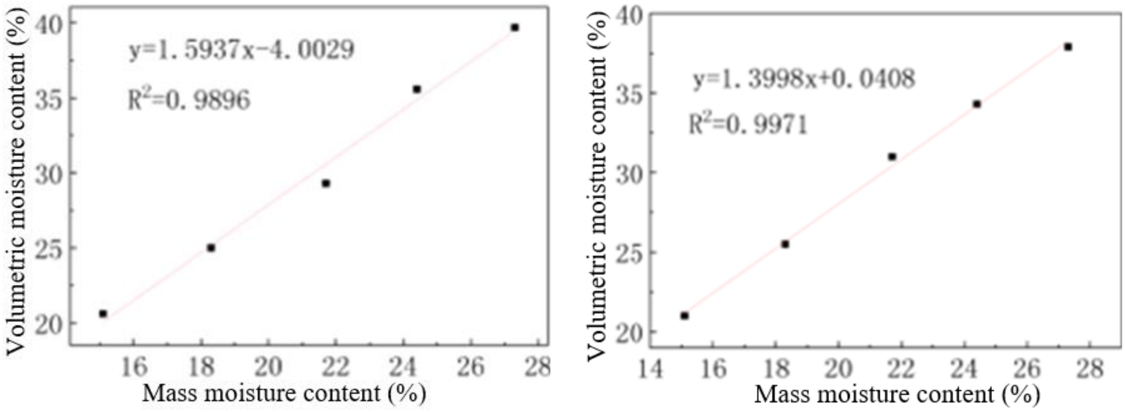

Figure 2. Conversion relationship between volumetric moisture content and mass moisture content

Table 3. Sensor temperature calibration results

Sensor Measured Temperature (℃)	-0.85	0.87	2.16	4.29	5. 1
Thermometer Measured Temperature (℃)	- 1.0	1.0	2.0	4.0	5.0

The volumetric moisture content and mass moisture content were plotted one-to-one, and the conversion relationship between the volumetric moisture content and mass moisture content was obtained, as shown in Figure 2.

For temperature calibration of the sensors, the soil sample was placed in a constant temperature chamber, and a thermometer was inserted into the soil sample. The temperature chamber was adjusted to different temperatures, and the soil sample was left to stand until its temperature stabilized. Then, the sensor was used to measure the temperature, and the thermometer reading was recorded. The measurement results are as follows.

From Table 3, it can be seen that the error between the sensor-measured temperature and the thermometer-measured temperature is less than 0.4℃, and the minimum reading of the thermometer is 1℃. Therefore, the temperature measurement of this sensor is accurate and can meet the requirements for moisture-temperature measurement.

3.3 Embedding of moisture-temperature monitoring equipment

To comparatively analyze the different moisture-temperature conditions of the fill embankment, cut embankment, and cut-to-fill section embankment, three typical cross-sections were selected on the newly constructed left-line road of the expansion project, with a uniform embankment height of 3 meters. These sections are the cut embankment at stake number K1204 + 360 (which contains a drainage trench), the fill embankment at stake number K1203 + 616 (which does not contain a drainage trench), and the fill embankment at stake number K1191 + 200 (which contains a drainage trench and is a cut-to-fill section). To obtain the distribution of the temperature field and moisture field within the embankment, sensors were arranged in four rows and two columns. In the transverse direction, the spacing between the two columns is 5 meters, with the outer column located 2.5 meters from the road edge. In the vertical direction, considering the structural differences between the cut and fill embankments, the sensors should be arranged separately. At stake number K1204 + 360, which is a cut section, sensors are installed at the top surface of the replacement gravel, 20 cm above the bottom surface of the replacement gravel, 20 cm below the top surface of the subgrade, and at a position 3 meters deep from the road surface within the subgrade. At stake numbers K1203 + 616 and K1194 + 200, which are fill sections, sensors are installed at the bottom surface of the 20 cm thick sand cushion layer, 20 cm above the bottom surface of the replacement gravel, 20 cm below the top surface of the subgrade, and at a position 3 meters deep from the road surface within the subgrade.

During on-site embedding, the lateral distance was measured at the corresponding stake number for pinpointing, the position was marked, and a hole was drilled on the road surface to a depth of 3 meters. Sensors were inserted into the sidewall of the hole from deep to shallow so that the sensor probes were fully embedded into the soil. After inserting the four sensors in the hole, the embankment soil was backfilled according to the original structural form, and the top layer was sealed with cement. The wires connected to the sensors were connected in parallel to the laterally arranged wires. Laterally, a groove was cut in the road surface, and the wires were placed in it and the groove was smoothed with cement mortar to prevent the wires from being exposed and damaged. Finally, the wires were connected to the power supply system and data transmission module, forming the moisture-temperature monitoring system.

4. RESULTS

4.1 Analysis of embankment temperature monitoring results

The monitoring point 1 of this highway project is located at stake number 1204 + 360. The figure below shows the temperature changes over time at different positions within the embankment from August 2021 to April 2022 (refer to Figure 3).

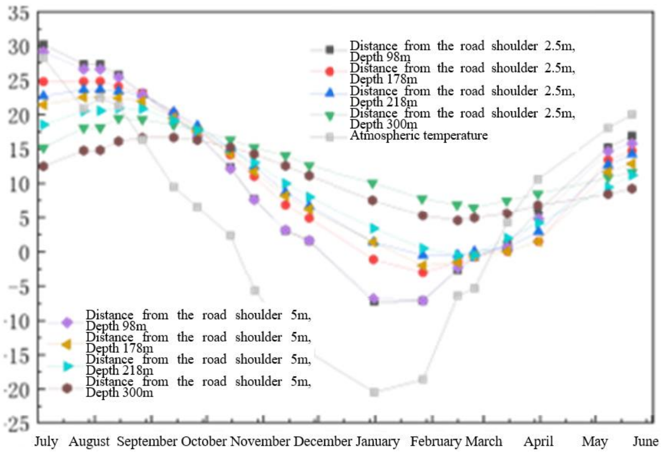

Figure 3. Temperature changes at different embankment positions and atmospheric temperature

(1) The temperature changes at different positions within the embankment are similar to the atmospheric temperature changes, showing a periodic sinusoidal pattern but with a certain lag. The temperature extremes and rates of temperature change at different positions within the embankment vary significantly.

At a depth of 98 cm below the road surface, the embankment temperature continuously decreased from July 2021 to January 2022 as the atmospheric temperature significantly dropped. At a depth of 178 cm below the road surface, the temperature remained relatively constant from late July to mid-August, with the temperature at 2.5 m from the road shoulder remaining at 24.8℃ and at 7.5 m from the road shoulder at 22℃. Subsequently, the temperature at 2.5 m from the road shoulder began to drop first, while the temperature at 7.5 m from the road shoulder did not start to decrease until early September. By late January 2022, the temperature at 2.5 m from the road shoulder had dropped below 0℃, while the temperature at 7.5 m from the road shoulder was around 1℃.

At a depth of 218 cm below the road surface and 2.5 m from the road shoulder, the temperature slightly increased by about 1℃ from late July to mid-August, reaching a peak of 23.7℃, after which it transitioned from an endothermic state to an exothermic state, reaching around 1℃ by late January 2022. At a depth of 218 cm below the road surface and 7.5 m from the road shoulder, the temperature rose from 18.5℃ in late July to 20.8℃ in mid-September. It then transitioned from an endothermic to an exothermic state, with the temperature dropping to around 3℃ by late January 2022. At a depth of 300 cm below the road surface, the temperature initially rose significantly and then decreased sharply. The temperature at 2.5 m from the road shoulder rose from 15.2℃ in late July to a maximum of 19.4℃ in early September, then dropped to 10.1℃ by late January 2022. The temperature at 7.5 m from the road shoulder reached a maximum of 16.7℃ in early October and decreased to 7.5℃ by late January 2022. After January, the atmospheric temperature began to rise, while the embankment temperature continued to drop until it began to rise from February to March. By April, the embankment temperature at the monitored positions had all risen to positive values, indicating that the frozen soil below a depth of 98 cm had completely thawed.

(2) The annual temperature variation amplitude at different positions within the embankment gradually decreases with depth. At 2.5 m from the road shoulder, the temperature variation amplitude decreases from 37.5℃ at a depth of 98 cm below the road surface to 9.34℃ at a depth of 300 cm. At 7.5 m from the road shoulder, the variation decreases from 35.96℃ at a depth of 98 cm below the road surface to 9.1℃ at a depth of 300 cm. This reflects the process of heat attenuation as it transfers downward within the embankment.

The depth at which the annual ground temperature variation amplitude is less than or equal to ± 0.1℃ is referred to as the annual ground temperature variation depth. The ground temperature at this depth is known as the average ground temperature. Below this depth, the ground temperature within the soil body generally does not change with time and can be considered a stable temperature field. According to the measured data from relevant scholars, the annual ground temperature variation depth is 10 m. A regression analysis combining the measured temperature data and the annual ground temperature variation depth results in Figure 4.

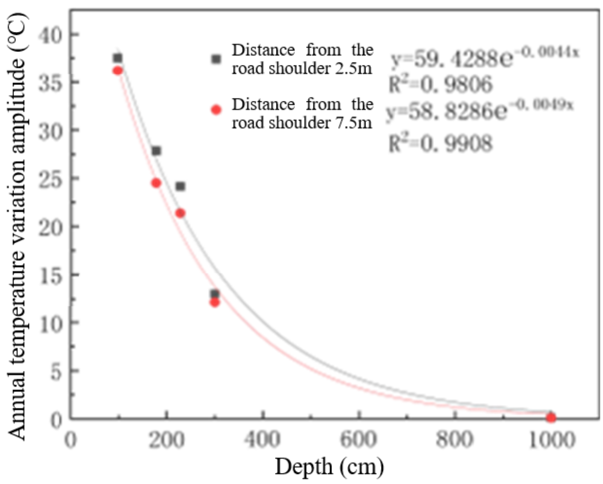

Figure 4. Temperature variation amplitude at different embankment positions

It can be seen that the exponential function has a good fit, and the temperature variation amplitude changes non-linearly with depth. The closer to the road surface, the greater the temperature variation. Moreover, the temperature variation amplitude at 2.5 m from the road shoulder decreases more rapidly with depth, indicating that the embankment temperature closer to the outer side is more susceptible to external environmental influences, while the internal temperature is more stable.

(3) The distribution of the temperature field in different seasons has distinct characteristics (refer to Figure 5). In summer, heat continuously transfers from the road surface into the embankment, resulting in a decreasing trend in temperature with increasing embankment depth; the closer to the road surface, the higher the embankment temperature. In autumn, as the ambient temperature gradually decreases, the low temperature begins to transfer downward from the road

surface. At a depth of 98 cm at 2.5 m and 7.5 m from the road shoulder, the temperatures drop to 17.2°C and 16.8°C, respectively. However, due to the difficulty of dissipating the accumulated heat within the embankment, there is a lag in the temperature change. As a result, at depths of 178 cm and 218 cm, the temperatures exceed 17.5°C. At deeper positions, the heat attenuates with depth and does not easily affect the temperature there, so at depths from 2.2 m to 3 m, the temperature decreases with depth. Overall, the embankment temperature shows a trend of first rising and then falling with increasing depth.

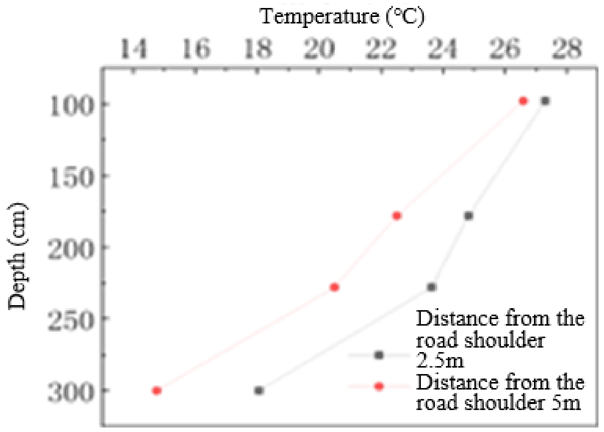

(a) Embankment temperature field on August 14 (summer)

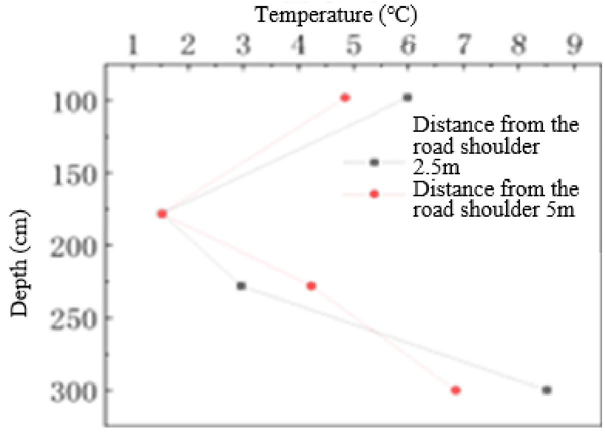

(b) Embankment temperature field on October 15 (autumn)

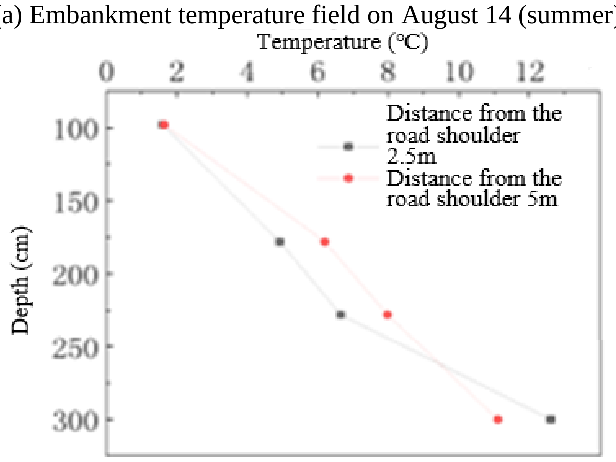

(c) Embankment temperature field on December 15 (winter)

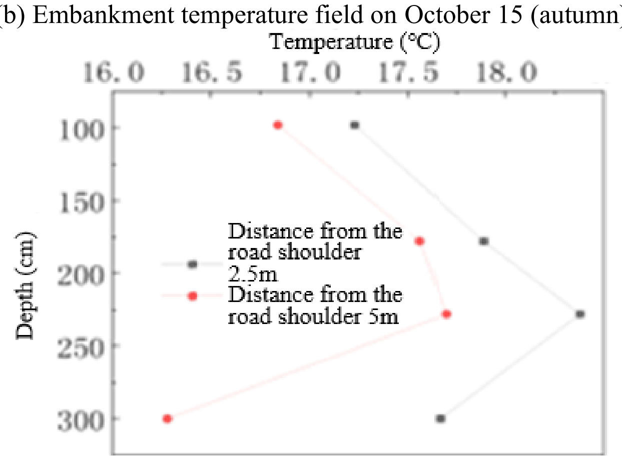

(d) Embankment temperature field on April 19 (spring)

Figure 5. Distribution patterns of temperature fields in different seasons

In winter, the ambient temperature is relatively low, and heat within the embankment continuously dissipates outward, resulting in a continuous increase in temperature with depth. In spring, the upper layer temperature of the embankment increases due to the rise in ambient temperature, but the temperature in the middle layer (1.5-2.5 m) has not yet changed and remains relatively low. The temperature at a depth of 3 m in the embankment is not easily affected by the external temperature, so the fluctuation is small. The embankment shows a trend of first decreasing and then increasing from top to bottom.

(4) Changes in Freezing Depth during the Frost Heave Period

The temperature data inside the embankment was fitted to obtain the temperature variation curves with depth at different times, thereby determining the depth below the road surface where the temperature is 0°C. This depth is referred to as the road freezing depth.

Figure 6 shows the development of freezing depth from November 8, 2021, to March 15, 2022. The embankment entered a frozen state in early November. Between early November and mid-December, the freezing depth developed slowly, with the freezing depths at both locations remaining consistent. From mid-December to late January 2022, the freezing depth developed rapidly, and there was a significant difference in the freezing depths at the two locations. The freezing depth at 2.5 m from the road shoulder reached 2 m, while at 7.5 m from the road shoulder, it was 1.6 m. From mid-February to mid-March, the freezing depths at both locations remained basically unchanged.

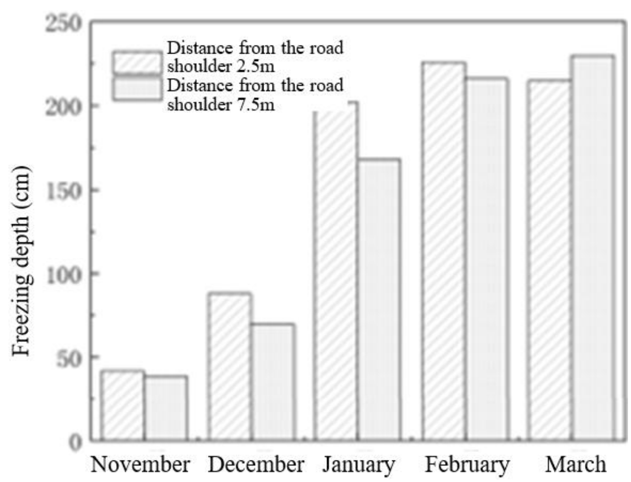

Figure 6. Variation of freezing depth over time

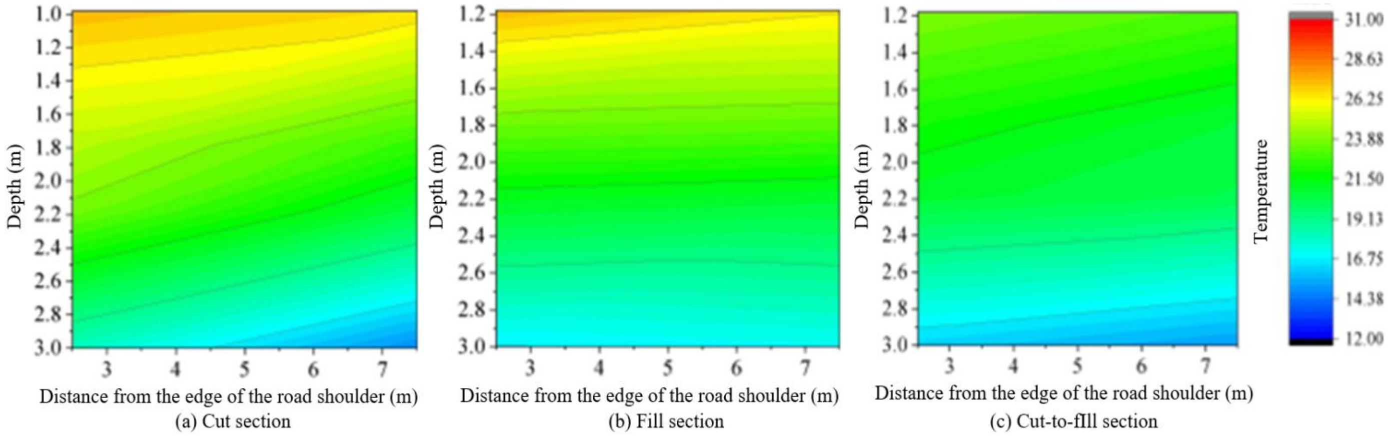

Figure 7. Distribution of temperature fields at different cross-sections

(5) Distribution of Embankment Temperature Fields under Different Cross-Sectional Forms

For the three monitored cross-sections, the temperature data for the same day in mid-August 2021 is plotted as shown in Figure 7.

Comparing the cut section and the fill section, the temperature lines in the cut section are more numerous and inclined, indicating that at the same depth, the temperature is higher near the road shoulder than near the center of the road, and there is a greater temperature difference within a depth range. In contrast, the temperature lines in the fill section are fewer and more horizontal, indicating that the temperature difference is not significant both laterally and vertically.

At a depth of 3 m near the center of the road, the embankment temperature in the cut section is lower, at 14.8°C. Comparing these three sections, the temperature at a depth of 3 m in the cut-to-fill section is closer to that in the cut section, but there is a smaller temperature difference within the measured depth range. This indicates that the cut-to-fill measures can effectively change the internal temperature distribution of the embankment, resulting in a more uniform temperature distribution and smaller temperature differences both laterally and vertically.

4.2 Analysis of embankment moisture monitoring results

(1) Variation patterns of the embankment moisture field

Due to the damage to some sensors during monitoring, some data were discarded. The volumetric moisture content was converted to mass moisture content based on the results of the sensor calibration experiments. The measured values are shown in Figure 8.

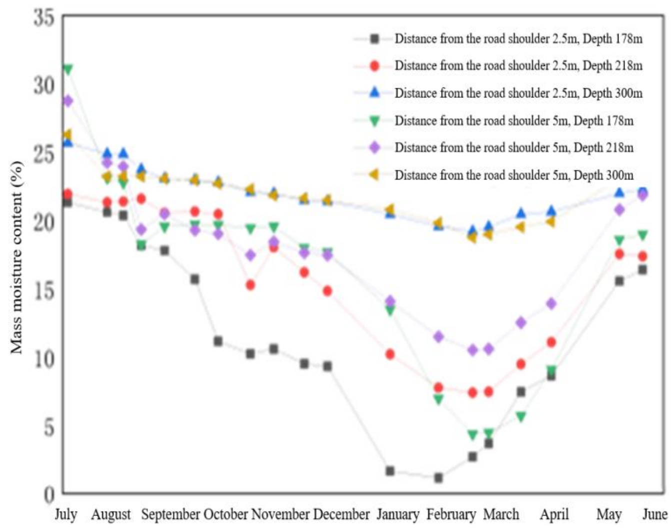

Figure 8. Measured values of embankment mass moisture content changes

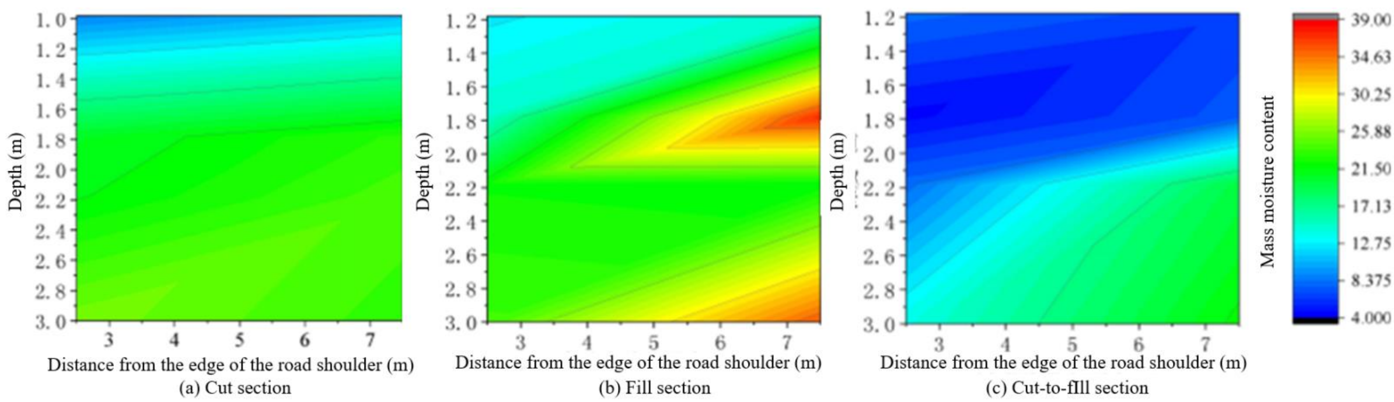

Figure 9. Distribution patterns of moisture fields at different cross-sections

(2) Moisture distribution patterns of different cross-sectional forms

The moisture distribution characteristics of the three selected cross-sectional forms are shown in Figure 9. The overall moisture content of the embankment in the cut section and cut-to-fill section is significantly lower, and at the same depth, the moisture content on the side closer to the road shoulder is lower. For the same position at 2.5 m from the road shoulder edge and a depth of 1.78 m, the moisture content of the cut section embankment is 20.68%, the moisture content of the cut-to-fill section embankment is 4.48% (which is 0.2 times that of the cut section), and the moisture content of the fill section embankment is 14.91% (which is 0.7 times that of the cut section). This indicates that the drainage trench set on the side of the road shoulder has a significant drainage effect. As the depth of the embankment increases, the moisture content gradually increases, which is caused by the rise of groundwater into the embankment under the influence of capillary action. Comparing the cut section and the cut-to-fill section, the overall moisture content of the embankment in the fill section is lower, mainly because the water on both sides of the slope of the cut embankment will migrate to the embankment under gravitational potential energy, while the slope of the fill embankment will continuously evaporate moisture under sunlight and air circulation [20, 21].

5. DISCUSSION

To analyze the moisture and temperature conditions of the embankment, this study selected three typical cross-sections of the highway and embedded sensors capable of real-time monitoring of embankment moisture and temperature. The data collected were then transmitted to a backend server using the IoT. The sensitivity and accuracy of the moisture and temperature measurements of the sensors were verified through laboratory calibration experiments, and the conversion formula between volumetric moisture content and mass moisture content was determined. This allowed the measured moisture data to be converted to the commonly used mass moisture content for moisture field analysis. Based on the temperature and moisture data of the embankment, the variation patterns were analyzed from both temporal and spatial perspectives, leading to the following conclusions:

(1) The temperature changes at different positions within the embankment are generally consistent with atmospheric temperature changes, showing a periodic sinusoidal pattern but with a certain lag. The temperature extremes and rates of temperature change at different positions within the embankment vary significantly. The embankment temperature reaches its maximum in August and its minimum between February and March. The annual variation amplitude of embankment temperature is nonlinearly negatively correlated with depth. The fitted curve for the annual temperature variation amplitude with depth at 2.5 m from the road shoulder edge is y=59.4288e-0.0044x, while at 5 m from the road shoulder edge, it is y=58.8286e-0.0049x.

(2) The temperature field of the embankment varies significantly across different seasons: in summer, the embankment temperature decreases with depth; in autumn, the embankment temperature first increases and then decreases with depth; in winter, the embankment temperature increases with depth; and in spring, the embankment temperature first decreases and then increases with depth.

(3) The moisture content of the embankment increases with depth, with the moisture content on the inner side of the embankment being greater than on the outer side. The moisture content of the embankment reaches its maximum in July and its minimum between January and March, showing a periodic variation of first decreasing and then increasing from July to June of the following year. Within a depth of 2.18 m below the road surface, the embankment moisture content varies with the cumulative monthly rainfall, but there is a lag. This indicates that the moisture content of the embankment is influenced by rainfall, but this influence gradually weakens with increasing embankment depth. By comparing the moisture content at the same position, it was found that the moisture content on the side closer to the road shoulder of the embankment with drainage trenches is significantly lower than that without drainage trenches, indicating that drainage trenches can effectively reduce the moisture content within the embankment.

6. CONCLUSION

This study conducted long-term monitoring of the distribution of moisture and temperature in the roadbed of highways in cold regions, revealing the patterns of temperature and moisture variations with depth and season. The monitoring results confirm that the temperature and moisture content of the roadbed are closely related to atmospheric conditions, exhibiting periodic patterns, which significantly impact the integrity and functionality of the roadbed structure.

These findings provide a scientific basis for optimizing the design and maintenance strategies of highways in cold regions, particularly in improving drainage systems and selecting suitable roadbed materials. Future research could further explore how to utilize these monitoring data to predict and prevent pavement diseases, thereby extending the lifespan of highways and enhancing their safety.

ACKNOWLEDGMENT

This paper was supported by Heilongjiang Provincial Innovation Training Project (Grant No.: S202310225029).

REFERENCES

[1] Kojima, Y., Nakano, Y., Kato, C., Noborio, K., Kamiya, K., Horton, R. (2020). A new thermo-time domain reflectometry approach to quantify soil ice content at temperatures near the freezing point. Cold Regions Science and Technology, 174: 103060. https://doi.org/10.1016/j.coldregions.2020.103060

[2] Fan, W., Yang, Z.J., Yang, P. (2020). A model for evaluating settlement of clay subjected to freeze-thaw under overburden pressure. Cold Regions Science and Technology, 173: 102996. https://doi.org/10.1016/j.coldregions.2020.102996

[3] Wang, T.L., Zhang, Y.Z., Wei, M., Cheng, B.Y., Wen, A. (2019). Investigation of liquid and vapor migration in coarse-grained soil during open-system step-freezing test. Cold Regions Science and Technology, 165: 102816. https://doi.org/10.1016/j.coldregions.2019.102816

[4] Yao, X., Wang, W., Zhang, M., Wang, S., Wang, L. (2021). Strain localization of a frozen sand under different test conditions. Cold Regions Science and Technology, 183: 103226. https://doi.org/10.1016/j.coldregions.2021.103226

[5] Stanier, S., Dijkstra, J., Leśniewska, D., Hambleton, J.,

White, D., Wood, D.M. (2016). Vermiculate artefacts in image analysis of granular materials. Computers and Geotechnics, 72: 100-113. https://doi.org/10.1016/j.compgeo.2015.11.013

[6] Saito, T., Yasuda, H., Sakurai, M., et al. (2016). Monitoring of stem water content of native and invasive trees in arid environments using GS3 soil moisture sensors. Vadose Zone Journal, 15(3): vzj2015-04. https://doi.org/10.2136/vzj2015.04.0061

[7] Kurylyk, B.L., Watanabe, K. (2013). The mathematical representation of freezing and thawing processes in variably-saturated, non-deformable soils. Advances in Water Resources, 60: 160-177. https://doi.org/10.1016/j.advwatres.2013.07.016

[8] Watanabe, K., Kito, T., Wake, T., Sakai, M. (2011). Freezing experiments on unsaturated sand, loam and silt loam. Annals of Glaciology, 52(58): 37-43. https://doi.org/10.3189/172756411797252220

[9] Liu, Z., Liu, J., Li, X., Fang, J. (2019). Experimental study on the volume and strength change of an unsaturated silty clay upon freezing. Cold Regions Science and Technology, 157: 1-12. https://doi.org/10.1016/j.coldregions.2018.09.008

[10] Bi, J., Zhang, M., Lai, Y., Pei, W., Lu, J., You, Z., Li, D. (2020). A generalized model for calculating the thermal conductivity of freezing soils based on soil components and frost heave. International Journal of Heat and Mass Transfer, 150: 119166. https://doi.org/10.1016/j.ijheatmasstransfer.2019.119166

[11] Tian, Z., Ren, T., Kojima, Y., Lu, Y., Horton, R., Heitman, J.L. (2017). An improved thermo-time domain reflectometry method for determination of ice contents in partially frozen soils. Journal of Hydrology, 555: 786-796. https://doi.org/10.1016/j.jhydrol.2017.10.055

[12] Striegl, A.M., Loheide II, S.P. (2012). Heated distributed temperature sensing for field scale soil moisture monitoring. Groundwater, 50(3), 340-347. https://doi.org/10.1111/j.1745-6584.2012.00928.x

[13] Konrad, J.M. (2008). Freezing-induced water migration in compacted base-course materials. Canadian Geotechnical Journal, 45(7): 895-909. https://doi.org/10.1139/T08-024

[14] Rakhimova, G., Stolboushkin, A., Vyshar, O., Stanevich, V., Rakhimov, M., Kozlov, P. (2023). Strong structure formation of ceramic composites based on coal mining overburden rocks. Journal of Composites Science, 7(5): 209. https://doi.org/10.3390/jcs7050209

[15] Hirose, G., Ito, Y., Ishikawa, T., Akagawa, S. (2017). Experimental prediction of permeability of freeze-thawed fine-grained soil. Journal of Japan Society of Civil Engineers, 73(2): 131-140. https://doi.org/10.2208/jscejge.73.131

[16] Yao, X., Zhang, M., Xu, G., Yu, F. (2018). Development of a novel plane strain test apparatus for frozen soils. Cold Regions Science and Technology, 155: 252-262. https://doi.org/10.1016/j.coldregions.2018.08.012

[17] Lu, Y., Shi, Y., Chen, B., Feng, Z., Hu, J. (2024). Structural damage characteristics and mechanism of granite residual soil. Applied Rheology, 34(1): 20240011. https://doi.org/10.1515/arh-2024-0011

[18] Paruta, A., Ciraolo, G., Capodici, F., et al. (2020). A geostatistical approach to map near-surface soil moisture through hyperspatial resolution thermal inertia. IEEE Transactions on Geoscience and Remote Sensing, 59(6): 5352-5369. https://doi.org/10.1109/TGRS.2020.3019200

[19] Kruse, A.M., Darrow, M.M. (2017). Adsorbed cation effects on unfrozen water in fine-grained frozen soil measured using pulsed nuclear magnetic resonance. Cold Regions Science and Technology, 142: 42-54. https://doi.org/10.1016/j.coldregions.2017.07.006

[20] Patterson, D.E., Smith, M.W. (1980). The use of time domain reflectometry for the measurement of unfrozen water content in frozen soils. Cold Regions Science and Technology, 3(2-3): 205-210. https://doi.org/10.1016/0165-232X(80)90026-9

[21] Patterson, D.E., Smith, M.W. (1981). The measurement of unfrozen water content by time domain reflectometry: Results from laboratory tests. Canadian Geotechnical Journal, 18(1): 131-144. https://doi.org/10.1139/t81-012